

Magneto-induced normal stress of magnetorheological plastomer

Taixiang Liu, Yangguang Xu, Xinglong Gong, Haoming Pang, and Shouhu Xuan

Citation: *AIP Advances* **3**, 082122 (2013); doi: 10.1063/1.4819462

View online: <http://dx.doi.org/10.1063/1.4819462>

View Table of Contents: <http://aipadvances.aip.org/resource/1/AAIDBI/v3/i8>

Published by the [AIP Publishing LLC](#).

Additional information on AIP Advances

Journal Homepage: <http://aipadvances.aip.org>

Journal Information: <http://aipadvances.aip.org/about/journal>

Top downloads: http://aipadvances.aip.org/features/most_downloaded

Information for Authors: <http://aipadvances.aip.org/authors>

ADVERTISEMENT

Explore AIP's open access journal:

- Rapid publication
- Article-level metrics
- Post-publication rating and commenting

Magneto-induced normal stress of magnetorheological plastomer

Taixiang Liu,^a Yangguang Xu,^a Xinglong Gong,^b Haoming Pang,
and Shouhu Xuan

CAS Key Laboratory of Mechanical Behavior and Design of Materials, Department of Modern Mechanics, University of Science and Technology of China, Hefei 230027, China

(Received 22 April 2013; accepted 12 August 2013; published online 21 August 2013)

An abrupt drop phenomenon of magneto-induced normal stress of magnetorheological plastomer is reported and a microstructure dependent slipping hypothesis is proposed to interpret this interesting behavior. For polyurethane based magnetorheological plastomer sample with 70 wt.% carbonyl iron powder, the magneto-induced normal stress can reach to as high as 60.2 kPa when a 930 mT magnetic field is suddenly applied. Meanwhile, the normal stress shows unpredicted abrupt drop. Particle dynamics is used to investigate the physical generating mechanism of normal stress. The simulation result agrees well with the experimental result, indicating that the interior microstructure of iron particle aggregation plays a crucial role to the normal stress. © 2013 Author(s). All article content, except where otherwise noted, is licensed under a Creative Commons Attribution 3.0 Unported License. [<http://dx.doi.org/10.1063/1.4819462>]

I. INTRODUCTION

Magnetorheological plastomer (MRP), which is prepared by dispersing micron-sized iron particles into a plasticine-like polymer matrix, is a new kind of smart magnetorheological materials and was reported in our previous work.^{1,2} MRP appears to be an interphase between magnetorheological fluid³ and magnetorheological elastomer.⁴ In the absence of external magnetic field the iron particles cannot move in the plastic matrix, but they can arrange or rearrange to form some chain-like microstructures along an applied magnetic field. This versatile characteristic makes MRP show a much higher magnetorheological effect than magnetorheological elastomer.¹ Except for novel performance in rheology, MRP can also overcome the headache particle sedimentation problem⁵ of magnetorheological fluid.

In regard to magnetorheological material, most investigations focus on the rheological effect in storage modulus, loss factor, stiffness, and some other magnetic field dependent properties.^{6,7} The pioneer works to normal force were reported by de Vicente *et al.*⁸ and See and Tanner,⁹ indicating that normal stress is sensitive to applied field under shear flow of magnetorheological fluid. Laun *et al.*¹⁰ investigated the primary and secondary normal stress differences of a magnetorheological fluid up to a 1.0 T magnetic field, showing that normal stress is important to stabilize concentricity in concentric cylinder arrangement. Recently, the normal stress issue re-catched the attentions of some researchers. The normal stress of magnetorheological fluid under one-way shear and oscillatory shear has been studied experimentally by Jang *et al.*¹¹ and Gong *et al.*,¹² respectively. Magneto-induced normal force of magnetorheological elastomer under compression state was investigated by Liao *et al.*¹³ Magneto-induced normal stress plays important role in the applications of magnetorheological material, such as polishing device, clutch, magneto-valve, seal device and especially the stability control of some magneto-device. Motivated by the aforementioned researches, for the new versatile

^aThe authors contributed equally to this work.

^bAuthor to whom correspondence should be addressed. Electronic mail: gongxl@ustc.edu.cn; Tel.: +86-551-63600419.

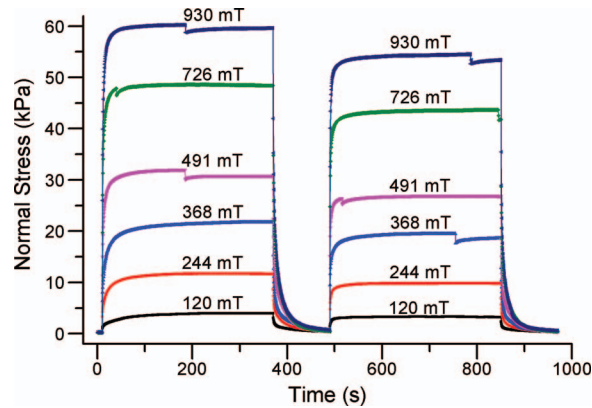


FIG. 1. The evolution of normal stress of MRP over time under different stepwise magnetic field. The incipient ten seconds record the initial state of test sample without magnetic field. Then external magnetic field is suddenly applied and the magnetic intensity is kept for six minutes. Then switch off the magnetic field and relax test sample. Two minutes later, the test procedure is repeated.

MRP with superior performance in rheology, we have investigated the interior magneto-induced normal stress and its microstructure-based generating mechanism. This paper will give a report specifically on an interesting abrupt drop phenomenon of magneto-induced normal stress of MRP.

II. EXPERIMENTAL

To explore the magneto-induced normal stress of MRP, a series of experiments were implemented at room temperature (25 Celsius degree). Test sample was polyurethane based MRP with 70 wt.% carbonyl iron particle (type CIP-CN, produced by BASF, Germany) which is prepared using the same method as was used in our previous work.¹ A commercial rheometer (type Physica MCR 301, produced by Anton Paar GmbH, Austria) with a magneto-controllable accessory (type MRD180) was used to test magneto-induced normal force. The test sample was imposed to the gap of upper plate (type PP20/MRD) and base bed, with parallel gap fixed as 1.000 mm to confine the vertical strain of test sample. The normal force is collected by the pressure sensor fixed on the upper plate and used to calculate the normal stress in the test sample.

As Fig. 1 shows, the normal stress can be greatly altered by an external magnetic field and the saturated normal stress increases accordingly with the increase of magnetic field. In particular, the normal stress can reach to as high as 60.2 kPa when suddenly applying a 930 mT magnetic field. The magneto-induced normal stress change is 3.44 times larger than the maximum normal stress change (17.5 kPa) of silicone rubber based magnetorheological elastomer with 80 wt.% carbonyl iron particle in the previous report by Liao *et al.*¹³

It can also be found from Fig. 1 that the normal stress gets a sudden increase and then approaches to saturated values slowly when an external magnetic field is applied. We regard this process as creep-like behavior of magneto-induced normal stress. The creep-like process in the forefront of loading stage shows complex nonlinear behavior with magneto-mechanical coupling. After the magnetic field is removed, the normal stress decreases gradually with time. Since the geometry of MRP is fixed by the parallel plate and the base bed of rheometer all the time, we can regard this process as the stress relaxation phenomenon of material. In addition, the normal stress in the posterior loading stage spends less time to get saturated than that in the previous loading stage and it is interesting that the saturate normal stress in posterior loading stage is smaller than that in the previous in a sequential test.

III. THEORETICAL ANALYSIS AND COMPUTATIONAL

Theoretical analysis and particle dynamic simulation are especially proposed to understand the microstructure-based generating mechanism of magneto-induced normal stress. To handle the

interaction of two iron particles, we introduce a modified magnetic interaction force \mathbf{F}_{ij}^m as an improvement to conventional magnetic dipole model. The force model is preferred for modeling the interaction of two close magnetized iron particles and presented as follow,

$$\mathbf{F}_{ij}^m = \begin{cases} c_m \times \mathbf{F}_{ij}^{dipole}, & \text{for } D \leq r \leq 1.5D \\ \mathbf{F}_{ij}^{dipole}, & \text{for } r > 1.5D \end{cases}, \quad (1)$$

$$c_m = 1 + \left(3 - \frac{2r}{D}\right)^2 \left(\frac{60.17}{1 + e^{(\theta-34.55)/12.52}} - 22.79\right) \frac{1}{100}, \quad (2)$$

$$\mathbf{F}_{ij}^{dipole} = -\frac{3\mu_0}{4\pi r^4 \mu_1} [(\mathbf{m}_i \cdot \mathbf{m}_j) \hat{\mathbf{r}} - 5(\mathbf{m}_i \cdot \hat{\mathbf{r}})(\mathbf{m}_j \cdot \hat{\mathbf{r}}) \hat{\mathbf{r}} + (\mathbf{m}_j \cdot \hat{\mathbf{r}}) \mathbf{m}_i + (\mathbf{m}_i \cdot \hat{\mathbf{r}}) \mathbf{m}_j], \quad (3)$$

where c_m is the correction factor for adjusting magnetic point dipole to model two close magnetized iron particles. $D = (d_i + d_j)/2$ is the average value of two considered particles' diameter d_i and d_j . \mathbf{r} is the position vector from particle i to particle j and $r = |\mathbf{r}|$, $\hat{\mathbf{r}} = \mathbf{r}/r$. θ denotes the angle of the direction external magnetic field and the relative position vector and the other constant coefficients are the fitting coefficients from data analysis. \mathbf{F}_{ij}^{dipole} is the well-known magnetic interaction force between two magnetic dipoles. In Eq. (3), μ_0 is the vacuum permeability; μ_1 is the relative permeability of matrix; \mathbf{m}_i and \mathbf{m}_j are the magnetic moment of particle i and j , respectively. More experimental and theoretical discusses can be found in such references.¹⁴ Excluded-volume force \mathbf{F}_{ij}^{ev} ¹⁵ and Van de Walls force \mathbf{F}_{ij}^{vdw} ¹⁶ are also taken into account for modeling the interaction of particle i and j . Due to carbonyl iron particle is made of soft magnetic material, the magnetic torque applied on particle is so small that the magneto-induced rotational motion of iron particle can be neglected. Hereto, the interaction force model between two iron particles is established.

We simplify the plastic polyurethane matrix as a Bingham fluid with initial yield shear stress τ_0 and dynamic viscosity η at a certain constant temperature. Then the viscous drag force applied on a moving particle i can be deduced as

$$\mathbf{F}_i^{drag} = -\frac{19\pi}{8} (d_i^2 \tau_0 \hat{\mathbf{v}} + d_i \eta \mathbf{v}), \quad (4)$$

where $\mathbf{v} = \frac{d\mathbf{r}}{dt}$ is the velocity of particle moving, and $\hat{\mathbf{v}}$ is the unit vector along \mathbf{v} . Inertia effect and stochastic motion of particle moving are not accounted, this proceeding is reasonable and discussed by Mohebi.⁷ With the forces aforementioned, the trajectory of particle i can be governed by kinematic equation

$$\begin{cases} \frac{d\mathbf{r}_i}{dt} = \frac{1}{\zeta_t} \left(\sum_{j \neq i} (\mathbf{F}_{ij}^m + \mathbf{F}_{ij}^{ev} + \mathbf{F}_{ij}^{vdw}) - \frac{19}{8} \pi d_i^2 \tau_0 \hat{\mathbf{v}} \right), & \text{for } \left| \sum \mathbf{F}_i \right| > \frac{19}{8} \pi d_i^2 \tau_0 \\ \frac{d\mathbf{r}_i}{dt} = \mathbf{0}, & \text{while } \left| \sum \mathbf{F}_i \right| \leq \frac{19}{8} \pi d_i^2 \tau_0 \end{cases}, \quad (5)$$

in which $\zeta_t = \frac{19}{8} \pi d_i \eta$ is the translational drag force coefficient and $\sum \mathbf{F}_i$ denotes the total force excluding the viscous drag force applied on particle i . Periodic boundary condition is applied and finite difference method is used to solve the kinematic equation. In the simulation, one time step is set as 0.001 second and the total computing time step has 5×10^5 steps. The computing time can cover the time range of a loading stage in experimental test. To calculate the interior stress state of MRP, a stress formula is introduced and presented as

$$\sigma_{\alpha\beta} = \frac{1}{V} \sum_{i=1}^{N-1} \sum_{j=i+1}^N r_{ij}^\alpha F_{ij}^\beta, \quad (6)$$

where V is the volume of considered cell, in which N particles are contained. r_{ij}^α is the distance along α direction (or axis) from particle i to j , and F_{ij}^β is the β direction component of interaction force of particle i to particle j .

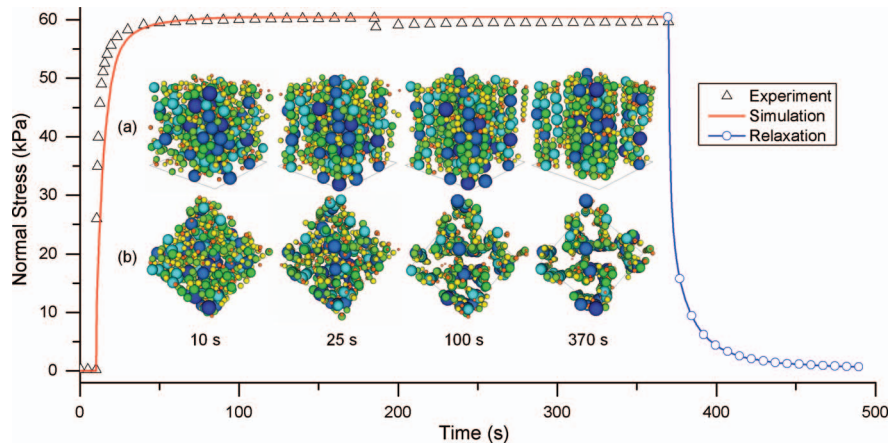


FIG. 2. Evolution of normal stress and relative interior microstructure changes over time under a 930 mT magnetic field. The internal illustrations show the microstructures at different time with axonometric views (a) and top views (b). The posterior stress relaxation curve is fitted from the experimental data.

IV. RESULTS AND DISCUSSION

In the simulation, the incipient 10 seconds are set to exclude volume overlap of particles randomly placed at original 0th second. To match the time range of experimental test, the simulation curve is cut at the 370th second and joints with a relaxation curve, which is fitted from the experimental data by using the KWW/Weibull function.¹⁷ As Fig. 2 shows, the simulation result agrees well with the experimental result, indicating the theoretical analysis is reasonable. Sudden increase is due to the instantaneous elasticity of matrix and iron particles aggregating some interior microstructures contributes to the creep-like process when suddenly applying an external magnetic field. Meanwhile, the microstructure evolution associating with the creep-like process of normal stress can be obtained: uniform dispersing at the 10th s, short chains at the 25th s, long chains at the 100th s, and vertical porous structure at the 370th s (along the direction of magnetic field). It is clear that the evolution of iron particle aggregating microstructure under an external magnetic field plays a crucial role for the creep-like process of normal stress. When applying magnetic field to initial isotropic sample in previous loading stage, particle-matrix interaction squeezes matrix vertically for the movement of iron particles driving by magnetic force and this will contribute to the normal stress. The matrix-induced normal stress will almost disappear in the relaxation stage. When the same magnetic field is applied to MRP again, the vertical porous microstructure aggregated by iron particles has already formed in the previous loading stage and the microstructure will be tensed while the matrix will not. Therefore, stable magneto-induced normal stress will generate directly in this stage and microstructure-matrix squeezing process will weakly happen. The above analysis explains why the normal stress in the posterior loading stage spends less time to get a stable state than that in the previous loading stage as well as the difference of the saturate value between two loading stages.

Abrupt drop phenomenon of normal stress in some loading stages can be observed in Fig. 1. It is found that the drop phenomenon certainly occurs when the magnetic intensity is larger than 491 mT and do not occur while the magnetic intensity is smaller than 244 mT. But the drop phenomenon of normal stress is not observed in the simulation result, which indicates that some new microstructure dependent mechanism has not been found. To understand the interesting phenomenon, a series of long time loading experiments were implemented. Here, we take the time-dependent normal stress under a 930 mT magnetic field for discussion.

It can be directly observed in Fig. 3 that the normal stress shows three abrupt drops at different time points. The normal stress gets sudden down at a drop point and then approaches to a larger value for a next drop point. Meanwhile, the intervals between drop points become larger and larger. Finally the normal stress gets a stable value with a very little perturbation and no drop happens again. It can be demonstrated that the abrupt drop phenomenon of normal stress occurs objectively, that is

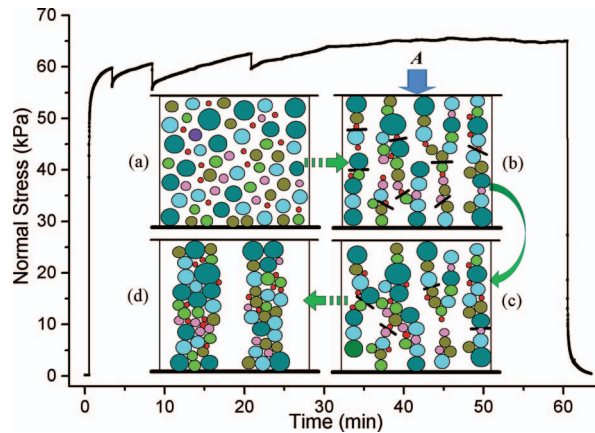


FIG. 3. Normal stress of MRP in response to a 930 mT magnetic field. The normal force of MRP was recorded in the incipient 30 seconds. Then the magnetic field was suddenly applied and kept for 60 minutes. Finally, the magnetic field was switched off and the test sample was relaxed for 3 minutes. The inset shows a schematic diagram: (a) initial isotropic state; (b) long chain-like structures with lots of unstable contact surfaces; (c) the state after some unstable contact surfaces crashing or slipping; (d) stable column-like structures. (—) represents the unstable contact surface and (A) represents the constraint reaction force.

the drop is not from some improper processing or instrumental error. Combining the experimental results in Fig. 1 and Fig. 3 with the simulation result in Fig. 2, it can be supposed that the interesting drop phenomena may originate from the rupture of chain-like structure due to friction and squeezing slip between contact particles. As the inset of Fig. 3 shows, when applying an external magnetic field, the uniform dispersed iron particles (Fig. 3(a)) aggregate some short chain-like structures near to each other firstly. In this process, small particles are attracted to large particles. Then some long chain-like structures are constructed by the short chains approaching to nearby others (Fig. 3(b)). However, these long chain-like structures are not stable enough as a result of that the contact surfaces between small particles and large particles in the long chains are easy to slip. When the value of tangential frictional force between contact particles exceeds a certain critical value, slipping occurs at the contact surface (Fig. 3(c)) and the rupture velocity of particle chains is suddenly larger than the reconstruction velocity of particle chains. This will result in the constraint reaction force, which is equivalent with the magnetic force of the particle chains and the extrusion force of matrix, drops down suddenly. Subsequently, the reconstruction velocity of particle chains is larger than the rupture velocity of particle chains, which makes the normal stress increase gradually with time until the next drop. Finally, the particles aggregate some stable column-like structures (Fig. 3(d)) and the normal stress reaches to a saturate value. The rupture and reconstruction process will make normal stress gets abrupt drop and approaches to a new value as well as the chain-like structure gets more and more stable. In addition, it is worth emphasizing that the rupture is a random-like process due to the complex particle distribution. For this reason, the drop phenomenon happens randomly and it is difficult to give a crucial magnetic intensity, which plays the role of watershed to determine whether the drop phenomenon occurs.

V. CONCLUSION

Three characteristics of magneto-induced normal stress of MRP are presented. Firstly, the normal stress of the MRP with 70 wt.% carbonyl iron powder can reach to as high as 60.2 kPa when suddenly applying a 930 mT magnetic field. The instability of normal stress appears when an moderate external magnetic field is applied. This issue should be paid attention to seriously in possible practical use. Secondly, theoretical analysis and relative numerical simulation reveal that the interior microstructure of iron particle aggregation plays a crucial role to the evolution of normal stress. Thirdly, a microstructure dependent slipping hypothesis can rationally explain the abrupt drop phenomenon of magnetic-field-induced normal stress and slip effect should be taken into account for

a more accurate simulation. This work is elementary to the exploration of the application of MRP, as well as the performance optimization of magnetorheological material and relative magneto-device design.

ACKNOWLEDGMENTS

Financial supports from the National Natural Science Foundation of China (Grant no. 11125210, 11102202) and the National Basic Research Program of China (973 Program, grant no. 2012CB937500) are gratefully acknowledged.

- ¹ Y. G. Xu, X. L. Gong, S. H. Xuan, W. Zhang, and Y. C. Fan, *Soft Matter* **7**, 5246 (2011).
- ² Y. G. Xu, X. L. Gong, S. H. Xuan, X. F. Li, L. J. Qin, and W. Q. Jiang, *Soft Matter* **8**, 8483 (2012).
- ³ D. T. Zimmerman, R. C. Bell, J. A. Filer, J. O. Karli, and N. M. Wereley, *Appl. Phys. Lett.* **95**, 014102 (2009); G. Bossis, S. Lacia, A. Meunier, and O. Volkova, *J. Magn. Magn. Mater.* **252**, 224 (2002); J. de Vicente, D. J. Klingenberg, and R. Hidalgo-Alvarez, *Soft Matter* **7**, 3701 (2011); M. T. López-López, L. Rodríguez-Arco, A. Zubarev, L. Iskakova, and J. D. G. Durán, *J. Appl. Phys.* **108**, 083503 (2010).
- ⁴ W. H. Li and X. Z. Zhang, *Smart Mater. Struct.* **19** (3) (2010); L. C. Davis, *J. Appl. Phys.* **85**, 3348 (1999); X. L. Gong, G. J. Liao, and S. H. Xuan, *Appl. Phys. Lett.* **100**, 211909 (2012).
- ⁵ I. B. Jang, H. B. Kim, J. Y. Lee, J. L. You, H. J. Choi, and M. S. Jhon, *J. Appl. Phys.* **97**, 10Q912 (2005).
- ⁶ X. J. Wang and F. Gordaninejad, *Rheol. Acta* **45**, 899 (2006); M. C. Heine, J. de Vicente, and D. J. Klingenberg, *Phys. Fluids* **18**, 023301 (2006); J. M. Ginder and L. C. Davis, *Appl. Phys. Lett.* **65**, 3410 (1994).
- ⁷ M. Mohebi, N. Jamasbi, and J. Liu, *Phys. Rev. E* **54**, 5407 (1996).
- ⁸ J. de Vicente, F. Gonzalez-Caballero, G. Bossis, and O. Volkova, *J. Rheol.* **46**, 1295 (2002).
- ⁹ H. See and R. Tanner, *Rheol. Acta* **42**, 166 (2003).
- ¹⁰ H. M. Laun, C. Gabriel, and G. Schmidt, *J. Non-Newton. Fluid Mech.* **148**, 47 (2008).
- ¹¹ J. L. Jiang, Y. Tian, D. X. Ren, and Y. G. Meng, *Smart Mater. Struct.* **20**, 085012 (2011).
- ¹² X. L. Gong, C. Y. Guo, S. H. Xuan, T. X. Liu, L. H. Zong, and C. Peng, *Soft Matter* **8**, 5256 (2012).
- ¹³ G. J. Liao, X. L. Gong, S. H. Xuan, C. Y. Guo, and L. H. Zong, *Ind. Eng. Chem. Res.* **51**, 3322 (2012).
- ¹⁴ C. Tan and T. B. Jones, *J. Appl. Phys.* **73**, 3593 (1993); E. E. Keaveny and M. R. Maxey, *J. Comput. Phys.* **227**, 9554 (2008); B. J. Cox, N. Thamwattana, and J. M. Hill, *Appl. Phys. Lett.* **88**, 152903 (2006); Z. Y. Wang, Z. Peng, K. Q. Lu, and W. J. Wen, *Appl. Phys. Lett.* **82**, 1796 (2003).
- ¹⁵ Sonia Melle, Oscar G. Calderón, Miguel A. Rubio, and Gerald G. Fuller, *J. Non-Newton. Fluid Mech.* **102**, 135 (2002).
- ¹⁶ D. J. Klingenberg, C. H. Olk, M. A. Golden, and J. C. Ulicny, *J. Phys.: Condens. Matter* **22**, 324101 (2010).
- ¹⁷ K. S. Fancey, *J. Mater. Sci.* **40**, 4827 (2005).